IOP Publishing Journal of Physics: Condensed Matter
J. Phys.: Condens. Matter **27** (2015) 054001 (8pp) doi:10.1088/0953-8984/27/5/054001

Reaction pathways for pyridine adsorption on silicon (0 0 1)

J M Bennett[1], N A Marks[2], J A Miwa[3], G P Lopinski[4], F Rosei[5], D R McKenzie[1] and O Warschkow[1]

[1] Centre for Quantum Computation and Communication Technology, School of Physics, The University of Sydney, Sydney, NSW 2006, Australia
[2] Discipline of Physics and Astronomy, Curtin University, Perth, WA 6845, Australia
[3] Department of Physics and Astronomy, Interdisciplinary Nanoscience Center (iNano), Aarhus University, 8000 Aarhus C, Denmark
[4] Measurement Science and Standards, National Research Council of Canada, Ottawa, Ontario K1A 0R6, Canada
[5] Institut National de la Recherche Scientifique, Énergie, Matériaux et Télécommunications, Varennes, Québec, J3X 1S2, Canada

E-mail: oliver@physics.usyd.edu.au

Received 17 August 2014, revised 5 October 2014
Accepted for publication 8 October 2014
Published 21 November 2014

Abstract

Density functional theory is used to describe the reactions of chemisorption of pyridine on the silicon (0 0 1) surface. Adsorption energies of six relevant structures, and the activation energies between them are reported. We consider in detail the dative to tight-bridge transition for which conflicting results have been reported in the literature, and provide a description of the formation of inter-row chains observed in high-coverage experiments. We demonstrate that the choice of DFT functional has a considerable effect on the relative energetics and of the four DFT functionals considered, we find that the range-separated hybrid ωB97X-D functional with empirical dispersion provides the most consistent description of the experiment data.

Keywords: pyridine, Si(0 0 1), density functional theory

(Some figures may appear in colour only in the online journal)

1. Introduction

Pyridine (C_5H_5N) is a quintessential heteroaromatic molecule and its reaction with the silicon (0 0 1) surface is of fundamental interest in the context of organically functionalized semiconductors and molecular electronics [1–5]. The reactivity of pyridine on Si(0 0 1) has been extensively studied both experimentally [6–12] and theoretically [6, 7, 12–19], and some of the key adsorption configurations are illustrated in figure 1 using previously unpublished scanning tunnelling microscopy (STM) images from the study described in [8]. In the initial stages of pyridine chemisorption onto Si(0 0 1) the lone pair on the nitrogen interacts with an electrophilic silicon atom to form a dative Si–N bond which preserves the aromaticity of the adsorbate. This species is observed in STM images as a single row-offset protrusion labelled DAT in figure 1(*a*) and the corresponding ball-and-stick structure is shown in figure 1(*c*). The consensus view is that from this initial configuration the adsorbate undergoes further reactions to yield one of two possibilities: a so-called tight-bridge configuration labelled TB1 in figures 1(*a*) and (*d*) which bridges between two adjacent dimers on the same row, and an inter-row structure labelled IR (figures 1(*b*) and (*e*)) which bridges between two dimers on adjacent rows. The inter-row structure tends to arrange into chains, involving multiple molecules bridging from one row to the next as seen in figure 1(*b*).

In this work we report a computational study to map out the absorption and reaction pathway of pyridine on Si(0 0 1) and clarify the competing pathways between on-row and inter-row structures. The experimental evidence strongly suggests that both the tight-bridge and inter-row configurations are

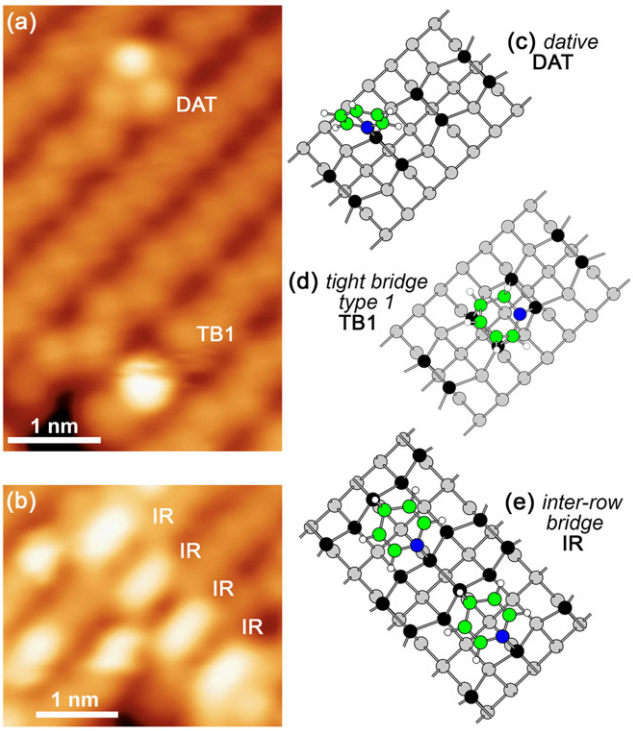

Figure 1. Principal adsorbate configurations arising from the exposure of pyridine to the Si(0 0 1) surface. (*a*, *b*) Filled-state STM images illustrating the initial adsorbate feature assigned to a dative (DAT) configuration, and two additional features arising from onwards reactions, which are assigned to the tight-bridge type 1 (TB1) and inter-row (IR) configurations. (*c*)–(*e*) Ball-and-stick representations of the corresponding structures. Note that a chain of only two IR adsorbates is shown in (*e*) whereas a chain of four IR is seen in the experimental image (*b*). Silicon atoms are shaded in black (surface) and grey (lower layers), carbon atoms in green, nitrogen in dark blue, and hydrogen in white. Imaging parameters in (*a*) and (*b*) are sample bias $U = -2.05$ V and a tunnelling current $I = 43$ pA.

Table 1. Absorption energies (eV) of selected pyridine structures from previous studies. The quantity $\Delta_{\text{TB1-DAT}}$ is the energy difference between the DAT and TB1 configurations, with a positive value indicating DAT is more stable.

Method	DAT	TB1	IR	$\Delta_{\text{TB1-DAT}}$	Reference
GGA/cluster	−1.17	−1.57	—	−0.40	[7]
GGA/slab	−1.17	−1.24	—	−0.07	[15]
GGA/slab	−1.40	−1.32	−1.01	+0.08	[16]
GGA/slab	−1.44	−1.15	−0.97	+0.29	[17]
GGA+D/slab	−1.80	−1.74	−1.64	+0.06	[17]
LDA/slab	—	—	—	−0.96	[14]

more stable than the dative precursor, but the corresponding theoretical literature is ambiguous as summarised in table 1. In particular, recent work by Coustel *et al* [16] and Ng *et al* [17] using density functional theory (DFT) in the generalised-gradient approximation (GGA) find that the datively bonded adsorbate is more stable than either the tight-bridge or the inter-row structure. In contrast, Kim and Cho [15] also use GGA-DFT and report the TB1 configuration to be slightly (0.07 eV) more stable than the dative configuration, in apparent agreement with experiment. Using the local density approximation (LDA) of DFT, Hong *et al* [14] find the tight-bridge configuration to be nearly 1 eV more stable than the dative configuration. Recently, we have observed [20] that the relative energy of these two pyridine structures on silicon (and two related configurations for benzene) is strongly dependent on the choice of density functional. Drawing on these results, we describe here the full reaction pathways of pyridine using the modern, range-separated hybrid ωB97X-D functional [21] that features long-range exact-exchange and an atom-pairwise empirical dispersion correction.

Our manuscript is structured as follows. In section 2 we introduce our composite model for calculating adsorption energies using cluster models of various sizes. In section 3 we present results for (A) the energetics of the principal adsorption configurations, (B) the reaction pathways leading to the formation of the TB1 configuration, and (C) the formation of the inter-row configurations. We conclude in section 4 with a discussion of the effects of the exchange-correlation functional.

2. Computational methodology

All calculations in this work are performed using cluster representations of the Si(0 0 1) surface and methods of energy computation, geometry optimisation and frequency calculation implemented in the Gaussian 09 software package [22]. Adsorption energies are calculated using a composite model approach [23–25] which manages the effects of finite cluster and basis set sizes. This approach involves an initial optimisation of a small cluster model that is subsequently corrected for basis-set-size, cluster-size and zero-point energy effects. This requires four separate calculations which are combined to give the final adsorption energy E for a given configuration as follows

$$E = E_{\text{initial}} + E_{\text{ZPC}} + E_{\text{BSC}} + E_{\text{CSC}} + E_{\text{align}} \qquad (1)$$

In this expression, E_{initial} is the initial geometry-optimized energy calculated using a small cluster model, a compact basis set (details below), and the high-level ωB97X-D density functional [21]. A zero point correction, E_{ZPC}, is obtained via a harmonic vibrational frequency calculation using the same combination of cluster, basis set and DFT functional. The optimized geometry for this cluster is used in a single point energy calculation with an extended basis set and the resulting energy used to determine a basis-set-size correction E_{BSC}. A cluster-size correction, E_{CSC}, is then obtained using the more economic B97D density functional [26] and two optimisations; one using the original small cluster and another using a larger cluster.

We use two sets of cluster models to describe on-row and inter-row reactions. For the on-row processes we combine a two-dimer, $Si_{15}H_{16}$ cluster (figure 2(*a*)) with a four-dimer $Si_{53}H_{44}$ cluster (figure 2(*b*)) as the respective small and large models in our composite approach. For the inter-row calculations the small model is a single-dimer, two-row $Si_{21}H_{24}$ cluster (figure 2(*c*)) while the large model is a three-dimer,

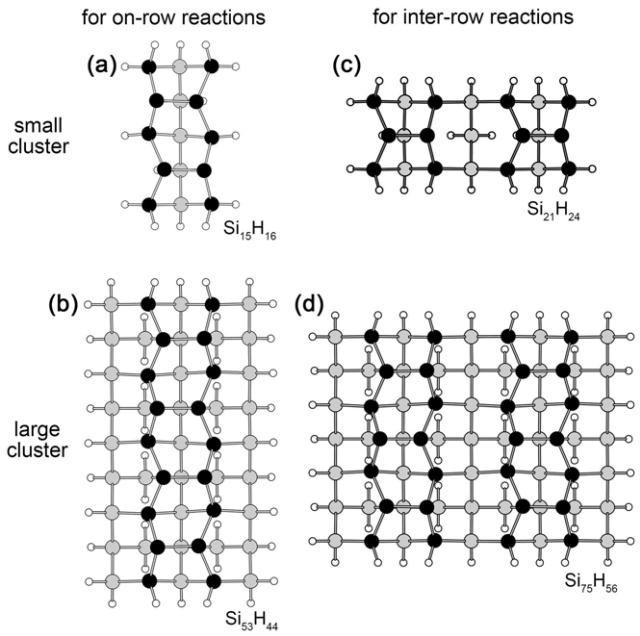

Figure 2. The clusters used to represent the Si(0 0 1) surface: (*a*) the single-row, two-dimer cluster ($Si_{15}H_{16}$), (*b*) the single-row, four-dimer cluster ($Si_{53}H_{44}$), (*c*) the two-row, two-dimer cluster ($Si_{21}H_{24}$) and (*d*) the two-row, six-dimer cluster ($Si_{75}H_{56}$). Silicon atoms are shaded in black (surface) and grey (lower layers), and cluster-terminating hydrogen atoms are shaded in white.

two-row $Si_{75}H_{56}$ (figure 2(*d*)) cluster. The fifth term in equation (1), E_{align}, is used to align the on-row and inter-row models on a common energy scale. This is achieved using the DAT adsorption energy as obtained by the single-row model as a reference; and the two-row model energies are shifted accordingly.

In the following we will also require a two-row cluster model with a single dangling bond defect, which we create by adding a single hydrogen atom. Energies obtained with this dangling-bond cluster model are aligned to those obtained with the non-defect, single-row model via the adsorption energy of the DAT structure. The assumption here is that the adsorption energy of the DAT structure is not affected by the presence of a dangling bond defect on the adjacent row.

The two basis sets, compact and extended, used in our composite model are defined as follows. The compact basis set consists of the 6-311++G(d,p) basis set for the atoms in the Si–Si dimers and the pyridine molecule, the 6-311G(d,p) basis set for the second layer of silicon atoms and the LANL2DZ pseudopotential for remaining layers of silicon atoms and the cluster-terminating hydrogen atoms. The extended basis set consists of the 6-311++G(2df,2pd) basis set for the molecule and Si–Si dimers and the 6-311G(2df,2pd) basis set for all other atoms.

In section 4 we examine the effect of the choice of functional. The same composite model as described above is also used for these calculations, except that the first three terms in equation (1) are evaluated with a different functional instead of ωB97X-D. The three functionals employed are the LDA [27], PW91 [28, 29], and B3LYP [30, 31] functionals.

3. Results

3.1. Structures

Figure 3 illustrates the main adsorption configurations considered in this work. In addition to the dative, tight-bridge and inter-row species seen experimentally (figure 1), we also consider three other species: an alternative tight-bridge (TB2; figure 3(*c*)), a 1,4-dimer-bridge structure, commonly referred to as butterfly (BF; figure 3(*d*)), and a 1,2-dimer-bridge structure (DB; figure 3(*e*)). With the exception of the latter, which is a high-energy intermediate, our calculated absorption energies for these structures are listed in table 2, along with previous values from the literature.

Looking first at our ωB97X-D results, we find that the TB1 configuration at −1.89 eV is slightly more stable than the DAT configuration (−1.87 eV) and while the energy difference is small (0.02 eV), this is in qualitative agreement with the experimental observations [8]. The BF configuration at −1.65 eV is significantly less stable than both DAT and TB1, while the alternative tight-bridge structure (TB2) is slightly less stable (by 0.08 eV) than TB1. This is consistent with STM experiments [8] which show no evidence of either the BF or the TB2 configurations. The inter-row structure at −2.13 eV is the most stable configuration and thus the observation of inter-row chains in experiment can be rationalised on thermodynamic grounds.

Comparing these results with earlier data we observe a number of trends. There is uniform consensus that the BF structure is less stable than DAT and that TB1 is preferred over TB2. Disagreement exists in the literature about the relative stability of DAT and TB1 as mentioned above, even though all four works are based on GGA density functionals. The calculations of Tao *et al* [7] and those of Kim and Cho [15] find that the TB1 structure is more stable by 0.40 and 0.07 eV, respectively, whereas Coustel *et al* [16] find the TB1 structure to be less stable by 0.08 eV. Ng *et al* [17] also find the TB1 structure to be less stable by 0.29 eV; this value is reduced to 0.06 eV when empirical dispersion corrections are included in their model. Switching to a GGA functional in our own calculations results in the same relative ordering as found by Coustel *et al* [16] and Ng *et al* [17] with an energy difference of 0.32 eV. One factor which complicates comparison of results is the orientation of the DAT structure in the calculations of Kim and Cho [15]. Their datively-bonded structure (figure 1 in [15]) is symmetrically constrained and hence not a true minimum. We compared this constrained configuration to the fully-relaxed configuration (figure 3(*a*)) and found[6] that the

[6] Using a two-row, six-dimer cluster $Si_{75}H_{56}$, the extended basis set (see text), and the same GGA functional (PBE) as used in [15], we find that the fully asymmetric dative configuration (figure 3(*a*)) is 0.15 eV more stable than the C(s)-symmetric dative structure described in [15] (see figure 1 in [15] where this structure is labelled EO). Vibrational frequency calculations confirm that the symmetric dative structure is not a true minimum, but a first-order saddle point, which suggests that the authors of [15] did not examine the stability of their dative structure with respect to symmetry breaking. This is significant because the authors of [15] report their dative structure to be 0.07 eV *less stable* than the TB1 tight bridge structure (labelled TBII in [15]). This means a full symmetry-breaking relaxation and a possible stability gain of 0.15 eV would have likely made their dative structure *more stable* than the tight bridge configuration, and thus in line with our GGA-DFT results, and those of Coustel *et al* ([16]) and Ng *et al* ([17]).

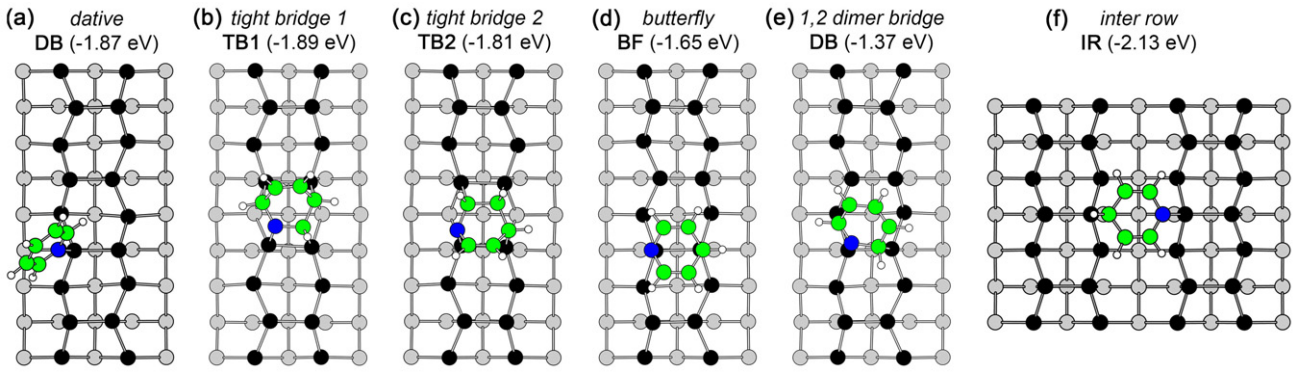

Figure 3. Top-view of the adsorbate structures relevant to this discussion. Silicon atoms are shaded in black (surface) and grey (lower layers), carbon atoms in green, nitrogen in dark blue, and hydrogen in white.

Table 2. Calculated adsorption energies in eV of pyridine on Si(0 0 1) in various configurations as illustrated in figure 3. Results from this work are compared with previous studies in the literature.

Method	DAT	TB1	BF	TB2	IR	Reference
GGA/cluster	−1.17	−1.57	−1.11	−1.31	—	[7]
GGA/slab	−1.17	−1.24	−0.82	−1.05	—	[15]
GGA/slab	−1.40	−1.32	−0.83	−1.09	−1.01	[16]
GGA/slab	−1.44	−1.15	−0.89	−0.94	−0.97	[17]
GGA+D/slab	−1.80	−1.74	−1.43	−1.53	−1.64	[17]
B3LYP/cluster	−1.17	—	−0.83	—	—	[13]
B3LYP/cluster	−1.40	—	−0.62	—	—	[6]
ωB97X-D/cluster	−1.87	−1.89	−1.65	−1.81	−2.13	This work
GGA/cluster	−1.58	−1.26	−1.02	−1.06	−1.30	This work

latter is lower in energy by approximately 0.15 eV in GGA-DFT. Taking this factor into account is likely to reverse the order of stability predicted in the work of Kim and Cho [15], and make it consistent with the GGA results of Coustel *et al* [16], Ng *et al* [17], and ourselves.

Regarding the inter-row structure, Coustel *et al* [16] find it to be less stable than the DAT structure by 0.39 eV, while Ng *et al* [17] report the same ordering with energy differences of 0.47 eV and 0.16 eV (without and with dispersion correction, respectively). These findings are in qualitative agreement with our GGA results where the difference is 0.28 eV. In contrast, our ωB97X-D calculations find that the IR structure is preferred, and is 0.26 eV more stable than the DAT structure. While the stability of the IR structure is superior with the ωB97X-D functional, one difference relative to earlier works is that the calculated adsorption energies are consistently larger (i.e. more negative). Using temperature programmed desorption (TPD) experiments, Li and Leung [6] report a desorption temperature of 520 K at low pyridine exposure and 430 K at high exposure. Using the Redhead equation [32], we can translate the desorption temperature into estimated adsorption energies of 1.4 ± 0.1 eV and 1.2 ± 0.1 eV, respectively[7]. This suggests that although the ωB97X-D functional predicts the correct relative stability, it is systematically overbinding the various adsorbates.

[7] This estimate uses the reported heating rate of 2 K s^{-1} and attempt frequencies in the range 10^{12} and 10^{14} Hz.

3.2. Reaction pathways

With figure 4 we consider the competing reaction pathways by which the DAT configuration reacts to form the TB1, TB2 and IR structures. Several schematic potential energy profiles are shown in this figure in which stationary points (stable structures, intermediates, and transition states) are indicated using horizontal bars. Transition states are further denoted by an asterisk and the rate-determining activation energies, E_A, are shown by vertical (red) arrows. The formation of the TB1 structure from DAT (see figure 4(*a*)) is a two-step process involving the 1,2 dimer bridge structure, DB, as an intermediate. The DB intermediate is less stable than both DAT and TB1 and is thus expected to be short-lived. Of the reaction steps, the first step (DAT→DB) has the higher activation energy of 0.96 eV relative to DAT and is therefore the rate-determining step. The second step (DB→TB1) has an activation barrier of 0.36 eV relative to DB, or 0.85 eV relative to DAT.

The formation of the competing TB2 structure (see figure 4(*b*)) also involves a two-step process in which the butterfly configuration, BF, is the intermediate. In contrast to the TB1 formation process, we see that the activation energies to form TB2 are significantly higher by approximately 0.5 eV. The rate-determining reaction is the second step between BF and TB2 with an activation energy of 1.49 eV relative to DAT. We note that the TB2 structure is slightly less stable than DAT so this process is overall endothermic.

In broad terms, these energy profiles are in agreement with the experimental observations. Firstly, the two-dimer

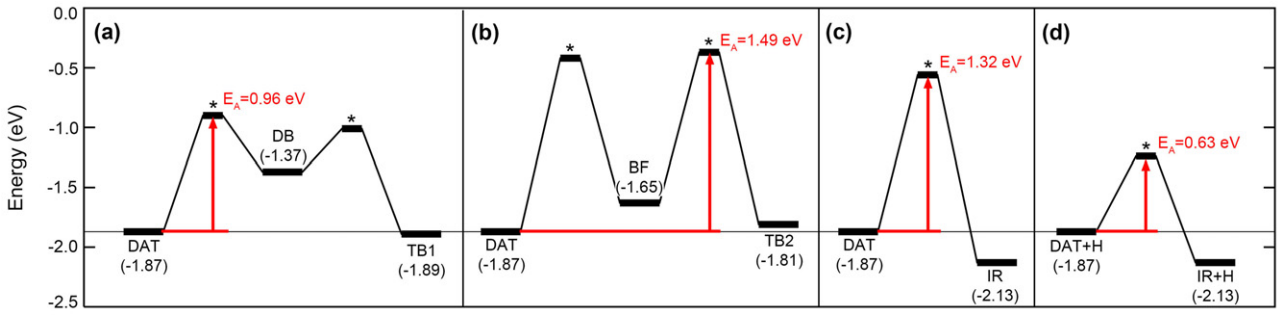

Figure 4. Calculated reaction profiles using the ωB97X-D cluster composite model between the DAT structure and the TB1, TB2, and IR structures. Adsorption energies (in eV) are indicated in brackets. For each path the rate-determining activation energy, E_A, is indicated using red arrows. For the DAT→IR reaction an additional profile (DAT+H→IR+H) is shown involving an additional hydrogen.

TB1 structure is energetically preferred (if only slightly) over the DAT structure, as observed in experiment. Secondly, the activation energy of 0.96 eV for the DAT→TB1 reaction is in excellent agreement with STM experiments [8] where counting statistics were used to estimate an activation barrier of ∼0.9 eV. Thirdly, the absence of the TB2 structure in experiments is explained by the high barrier of 1.49 eV which is kinetically prohibitive at room temperature with an estimated rate nine orders of magnitude smaller than that of the TB1 reaction.

Both these reaction paths have been previously studied by Kim and Cho [15] and also by Ng *et al* [17]. Our transition state energies in both reactions differ from these works, but we arrive at the same conclusion, namely that the formation of the TB1 structure is kinetically more favourable than the formation of the TB2 structure since it has a lower activation energy. The difference in the transition state energies most likely results from the use of different functionals and differing method for identifying the transition state. As will be discussed later, the choice of functional has a considerable effect on the relative energies of the structures for pyridine on Si(0 0 1).

3.3. Inter-row structures

In figure 4(*c*) we show the energy profile for the reaction of a DAT species to form a single inter-row bridge structure (IR). A ball-and-stick representation of this process, along with the transition state (labelled TS), is shown in figures 5(*a*)–(*c*). Even though this reaction breaks the aromaticity of the pyridine, a net energy gain of 0.26 eV is achieved. This suggests that the formation of the inter-row structures seen in experiment is thermodynamically driven. However, the calculated activation energy of 1.32 eV (see figure 4(*c*)) is too high for this particular reaction to play a significant role at room temperature. Ng *et al* [17] also consider this reaction using GGA-DFT. Their results differ from ours in two ways: they find a much lower activation energy and their IR structure is calculated to be less stable than DAT. This would imply that the DAT to IR reaction is kinetically accessible, but thermodynamically unfavourable, whereas we find the converse.

In figures 5(*d*)–(*f*) we consider an alternative inter-row reaction in which an additional hydrogen atom is present on the far end of the reacting free dimer. This configuration,

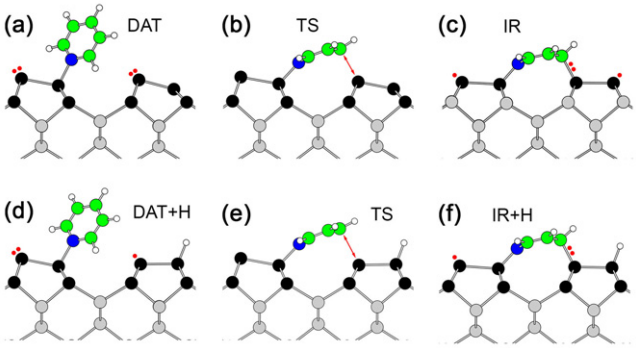

Figure 5. Structure views of the dative (DAT) to inter-row (IR) reaction with (*a*)–(*c*) a clean dimer and (*d*)–(*f*) a hemihydride defect on the adjacent row. Shown for both reactions are the initial and final structures as well as the transition state. Red dots are used to indicate the electron occupancy of the relevant dimer dangling bonds and the role of these electrons in creating the pyridine-silicon covalent bond.

nominally a hemihydride dimer, creates a dangling bond (see figure 5(*d*)) and mimics the presence of either a pre-existing defect or another inter-row structure. The energy profile for this second reaction is shown in figure 4(*d*). We see that the presence of the hydrogen leaves the relative energies between the initial and final state unchanged, but the barrier for the reaction is substantially reduced. With a barrier of 0.63 eV the reaction proceeds rapidly at room temperature, with a lifetime of milliseconds. This is orders of magnitude faster than the DAT to TB1 reaction, but we emphasise that this only occurs in the presence of a dangling bond on the adjacent row.

Experimental observations on inter-row features show these to occur predominantly in chains whereby successive IR structures are linked end-to-end to bridge over several rows (see figure 1(*b*)). The calculated barriers provide a simple rationalisation of this behaviour; IR structures can only form when there is a half-terminated dimer with a dangling bond on the adjacent row, such as those created by a C defect [33] or a hemihydride. Once a single IR structure has formed, it creates a new dangling bond which self-catalyses further IR reactions leading to the chains observed in experiments. In this aspect, the pyridine IR chain-growth mechanism is not dissimilar to the self-directed growth of styrene molecular chains on the (2 × 1) H:Si(0 0 1) surface [34].

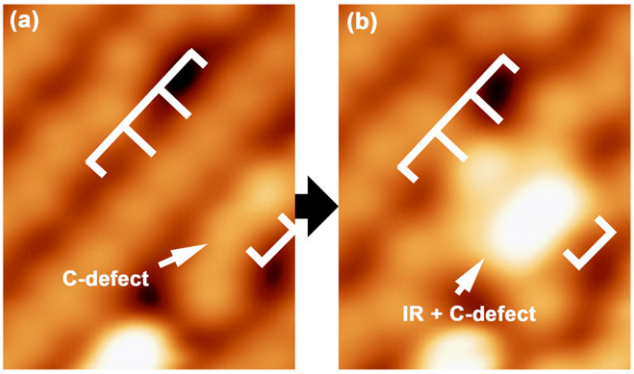

Figure 6. Sequence of two filled-state STM images showing a pyridine inter-row bridge forming at the site of a C defect. This is an experimental illustration of the dangling-bond facilitated reaction described in figures 5(*d*)–(*f*). The images were recorded using a sample bias $U = -2.05$ V and a set point current $I = 43$ pA.

An example of an inter-row feature forming at the site of a C defect is shown in figure 6. These defects arise from the dissociation of residual water molecules on the surface [35, 36] creating a two-dimer-wide defect composed of a Si–Si–H hemihydride dimer and a Si–Si–OH dimer. Each of these dimers contains a dangling bond, which appear as two characteristic protrusions offset from the dimer-row centre (see lower right corner in figure 6(*a*)). The same area imaged four minutes later while pyridine dosing continued shows the appearance of a bright inter-row protrusion (see figure 6(*b*)). The most plausible interpretation is that a pyridine molecule has landed on the adjacent row and has immediately reacted to form an IR structure. While it is unclear from the images whether the pyridine molecule reacted with the hemihydride or the OH dimer, it is reasonable to presume that the dangling bond of either dimer would facilitate the IR formation reaction.

Ng *et al* [17] also consider inter-row chain growth in their calculations and conclude that chain growth is driven by thermodynamic effects. While a single inter-row bridge is less stable than DAT in their model, they find that this order reverses as the inter-row chain grows in length. While increasing stability with chain length may well occur, we believe that our kinetic model provides a more natural interpretation for how inter-row chain growth is initiated. Further experimental studies will hopefully shed further light on the relative contribution of thermodynamic and kinetic factors governing inter-row chain growth.

4. Discussion and conclusion

In the introduction we highlighted the considerable disagreements that exist in the theoretical literature regarding the relative stability of the dative and tight bridge configurations. We believe these disagreements can be well understood as arising from sensitivity of this reaction system to the choice of exchange-correlation functional. This is illustrated by figure 7 which compares the absorption energies of the main configurations, DAT, TB1, and IR, as computed using four different functionals, namely, the local density approximation (LDA),

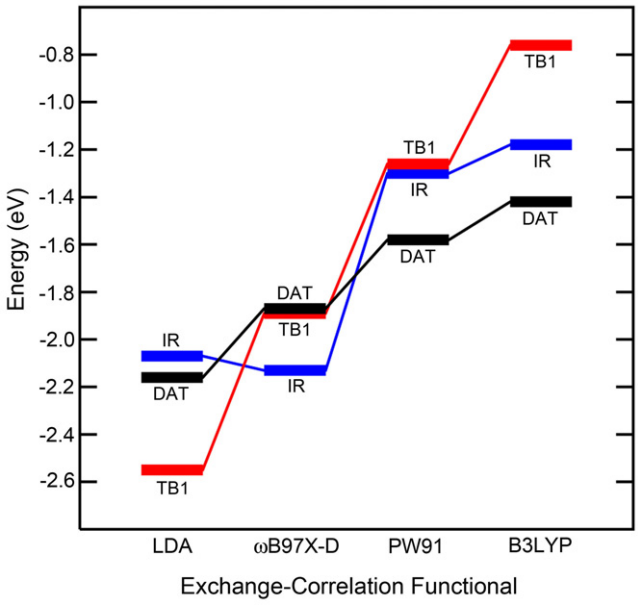

Figure 7. Absorption energy of the DAT, TB1 and IR structures calculated using the composite model with four different functionals: LDA [27], ωB97X-D [21], PW91 [28, 29], and B3LYP [30, 31]. All energies are expressed relative to the isolated gas-phase molecule and bare surface.

the generalised-gradient approximation (GGA; PW91 functional), the B3LYP hybrid functional, and ωB97X-D range-separated functional. We see that both the absolute adsorption energies and the relative stability of these configuration changes considerably with the choice of functional. For example, the most stable predicted configuration of the three is the TB1 structure for LDA, the dative structure for PW91 and B3LYP, and the IR structure for ωB97X-D. A similar situation exists for the least stable structure, with all three structures represented amongst the four functionals.

Of the four functionals presented, we believe that the ωB97X-D functional provides the best representation of the chemistry *on* the surface. According to PW91 and B3LYP the dative structure should not transform into TB1, as the latter is less stable. With the LDA, the TB1 structure is correctly predicted to be more stable than the dative structure, however the inter-row structure should not be seen as it is predicted to be less stable. Only with the ωB97X-D functional is the dative structure the least stable, and hence provides a thermodynamic driving force to form both inter-row and tight-bridge structures as observed experimentally [8].

Where the ωB97X-D functional performs less satisfactorily is in the absolute absorption energies which vary between -2.13 (IR) and -1.87 eV (DAT). This suggests considerable overbinding in comparison to an estimate of 1.4 ± 0.1 eV (see section 3.1) based on TPD experiments [6]. The overbinding is even more pronounced in the LDA. In contrast, the PW91 and B3LYP functionals compare quite well to the experimental estimate.

The sensitivity of the DAT to TB1 energy difference, $\Delta_{\mathrm{TB1-DAT}}$, to the choice of density functional can also be discerned in the previous literature (see table 1), keeping in mind that some of the reported differences are also affected

by other computational approximations. Our finding of a large preference for the TB1 configuration using the LDA is consistent with the earlier LDA results of Hong *et al* [14]. Similarly, our calculated preference for the DAT configuration using GGA exchange-correlation (see table 2) matches the earlier findings of Coustel *et al* [16] and Ng *et al* [17], who have both noted that this preference does not agree with experimental observations [8]. Coustel *et al* [16] and Ng *et al* [17] use a planewave approach and large surface unit cells which means their results, similar to ours, are likely to reflect the genuine performance of the GGA functional without being masked by other approximations, such as limited basis set size or slab/cluster size. This is not the case in the GGA calculations of Tao *et al* [7] and Kim and Cho [15] where the use of, respectively, a limited basis set and a symmetrically-constrained DAT structure result in a predicted preference for the TB1 configuration. As discussed above, these additional approximations have plausibly offset the intrinsic preference of the GGA functional for the pyridine DAT configuration.

Coustel *et al* [16, 19] propose a thermodynamic explanation based on a postulated entropy contribution associated with the aromatic ring to account for the apparent discrepancy between their GGA results and experimental observation. We feel this explanation relies too much on the assumption that GGA-DFT affords a qualitatively correct description of the 0 K energy difference. However, as highlighted in figure 7, the relative stability between DAT and TB1 is quite sensitive to how the effects of electron exchange and correlation are represented in DFT. The ωB97X-D functional is distinguished from the other three functionals in figure 7 by an empirical, atom-pairwise dispersion correction term and a full exact-exchange treatment in the long-range limit [21]. This suggests that these ingredients potentially play an important role in describing the energetics of the pyridine/Si(0 0 1) reaction system. However, one must also keep in mind that these four functionals differ considerably in how their internal parameterisation was arrived at. Specifically, the designers of the ωB97X-D functional have followed modern trends and used a very large data set of reference energies to fit the 18 internal parameters that define this particular functional (see [21] for details). This too could be a significant factor contributing to the better performance of the ωB97X-D functional. It would be premature at this point to single out any one of these factors as directly responsible for the observed sensitivity of the pyridine/Si(0 0 1) energetics with respect to the choice of density functional. This is the subject of further studies [20]. Meanwhile, we expect the pyridine on Si(0 0 1) system to be a useful test case for future functional development.

In summary, we have computed energy barriers and relative energetics for the chemisorption of pyridine on the silicon (0 0 1) surface. Our calculations correctly delineate between two competing pathways between the initial dative configuration and the thermodynamically more stable tight-bridge configuration. Using a kinetic argument based on dangling bonds created by pre-existing defects we explain the formation of inter-row chain structures observed in high-coverage experiments. We also show that the choice of functional has a large effect on both absolute and relative energies. While not perfect, we find that the range-separated ωB97X-D functional used in this work provides a description of the reaction system that is most consistent with the experimental evidence. Accordingly, we expect this functional to be of wider utility to study other reactions systems involving aromatic molecule adsorption on silicon.

Acknowledgments

OW, JMB and DRM are supported by the Australian Research Council Centre of Excellence for Quantum Computation and Communication Technology (CE110001027). NAM is supported by an Australian Research Council Future Fellowship (FT120100924). FR and GPL are supported by NSERC Discovery Grants. FR acknowledges partial salary support from the Canada Research Chairs program and is grateful to NSERC for an E W R Steacie Memorial Fellowship. FR thanks the A von Humboldt Foundation for a F W Bessel Award and Elsevier for a grant from Applied Surface Science. Computing support was provided by the Australian National Computational Infrastructure (NCI).

References

[1] Bent S F 2002 *Surf. Sci.* **500** 879
[2] Filler M A and Bent S F 2003 *Prog. Surf. Sci.* **73** 1
[3] Yoshinobu J 2004 *Prog. Surf. Sci.* **77** 37
[4] Leftwich T R and Teplyakov A V 2008 *Surf. Sci. Rep.* **63** 1
[5] Tao F F and Bernasek S L 2012 *Functionalization of Semiconductor Surfaces* (New York: Wiley)
[6] Li Q and Leung K T 2003 *Surf. Sci.* **541** 113
[7] Tao F, Qiao M H, Wang Z H and Xu G Q 2003 *J. Phys. Chem.* B **107** 6384
[8] Miwa J A, Eves B J, Rosei F and Lopinski G P 2005 *J. Phys. Chem.* B **109** 20055
[9] Coustel R and Witkowski N 2008 *J. Phys. Chem.* C **112** 14102
[10] Lee H-K, Kim K-J, Kang T-H, Kim S, Chung J W and Kim B 2008 *J. Electron Spectrosc. Relat. Phenom.* **164** 44
[11] Weier D, Lühr T, Beimborn A, Schönbohm F, Döring S, Berges U and Westphal C 2011 *Surf. Sci.* **605** 1784
[12] Coustel R, Carniato S, Rochet F and Witkowski N 2012 *Phys. Rev.* B **85** 035323
[13] Lu X, Xu X, Wu J, Wang N and Zhang Q 2002 *New. J. Chem.* **26** 160
[14] Hong S, Cho Y E, Maeng J Y and Kim S 2004 *J. Phys. Chem.* B **108** 15229
[15] Kim H-J and Cho J-H 2004 *J. Chem. Phys.* **120** 8222
[16] Coustel R, Carniato S and Boureau G 2011 *J. Chem. Phys.* **134** 234708
[17] Ng W K H, Liu J W and Liu Z-F 2013 *J. Phys. Chem.* C **117** 26644
[18] Romeo M, Balducci G, Stener M and Fronzoni G 2014 *J. Phys. Chem.* C **118** 1049
[19] Coustel R, Carniato S and Boureau G 2014 *J. Phys. Chem.* C **118** 17505
[20] Warschkow O, Bennett J M, Miwa J A, Lopinski G P, Rosei F, McKenzie D R and Marks N A 2014 in preparation
[21] Chai J-D and Head-Gordon M 2008 *Phys. Chem. Chem. Phys.* **10** 6615
[22] Frisch M J *et al* 2009 *GAUSSIAN 09, Revision D.01* (Wallingford CT: Gaussian)
[23] Warschkow O, McDonell T L and Marks N A 2007 *Surf. Sci.* **601** 3020

[24] Warschkow O, Gao I, Schofield S R, Belcher D R, Radny M W, Saraireh S A and Smith P V 2009 *Phys. Chem. Chem. Phys.* **11** 2747
[25] Tracey D F, Delley B, McKenzie D R and Warschkow O 2013 *AIP Adv.* **3** 042117
[26] Grimme S 2006 *J. Comput. Chem.* **27** 1787
[27] Vosko S H, Will L and Nusair M 1980 *Can. J. Phys.* **58** 1200
[28] Perdew J P, Chevary J A, Vosko S H, Jackson K A, Pederson M R, Singh D J and Fiolhais C 1992 *Phys. Rev.* B **46** 6671
[29] Perdew J P, Burke K and Wang Y 1996 *Phys. Rev.* B **54** 16533
[30] Becke A D 1993 *J. Chem. Phys.* **98** 5648
[31] Lee C, Yang W and Parr R G 1988 *Phys. Rev.* B **37** 785
[32] Redhead P A 1962 *Vacuum* **12** 203
[33] Hamers R J and Köhler U K 1989 *J. Vac. Sci. Technol.* A **7** 2854
[34] Lopinski G P, Wayner D D M and Wolkow R A 2000 *Nature* **406** 48
[35] Yu S-Y, Kim H and Koo J-Y 2008 *Phys. Rev. Lett.* **100** 036107
[36] Warschkow O, Schofield S R, Marks N A, Radny M W, Smith P V and McKenzie D R 2008 *Phys. Rev.* B **77** 201305